10-1-2002

Effect of Hydrophobic Surfactant Proteins SP-B and SP-C on Phospholipid Monolayers. Protein Structure Studied Using 2D IR and βν Correlation Analysis

Saratchandra Shanmukh
University of Georgia

Phillip Howell
University of Georgia

John A. Baatz
Medical University of South Carolina

Richard A. Dluhy
Medical University of South Carolina

Effect of Hydrophobic Surfactant Proteins SP-B and SP-C on Phospholipid Monolayers. Protein Structure Studied Using 2D IR and $\beta\nu$ Correlation Analysis

Saratchandra Shanmukh,* Phillip Howell,* John E. Baatz,† and Richard A. Dluhy*
*University of Georgia, Department of Chemistry, Athens, Georgia 30602-2556 and †Medical University of South Carolina, Department of Pediatrics, Charleston, South Carolina 29425 USA

ABSTRACT We have applied two-dimensional infrared (2D IR) and $\beta\nu$ correlation spectroscopy to in-situ IR spectroscopy of pulmonary surfactant proteins SP-B and SP-C in lipid–protein monolayers at the air—water interface. For both SP-B and SP-C, a statistical windowed autocorrelation method identified two separate surface pressure regions that contained maximum amide I intensity changes: 4–25 mN/m and 25–40 mN/m. For SP-C, 2D IR and $\beta\nu$ correlation analyses of these regions indicated that SP-C adopts a variety of secondary structure conformations, including α-helix, β-sheet, and an intermolecular aggregation of extended β-sheet structure. The main α-helix band split into two peaks at high surface pressures, indicative of two different helix conformations. At low surface pressures, all conformations of the SP-C molecule reacted identically to increasing surface pressure and reoriented in phase with each other. Above 25 mN/m, however, the increasing surface pressure selectively affected the coexisting protein conformations, leading to an independent reorientation of the protein conformations. The asynchronous 2D IR spectrum of SP-B showed the presence of two α-helix components, consistent with two separate populations of α-helix in SP-B—a hydrophobic fraction associated with the lipid chains and a hydrophilic fraction parallel to the membrane surface. The distribution of correlation intensity between the two α-helix cross peaks indicated that the more hydrophobic helix fraction predominates at low surface pressures whereas the more hydrophilic helix fraction predominates at high surface pressures. The different SP-B secondary structures reacted identically to increasing surface pressure, leading to a reorientation of all SP-B subunits in phase with one another.

INTRODUCTION

Mammalian pulmonary surfactant is a highly specialized substance that contains approximately 85% phospholipid, 7–10% protein, and 4–8% neutral lipid (Creuwels et al., 1997; Notter, 2000). The most abundant phospholipid class is phosphocholine, whereas anionic phospholipids including phosphoglycerols make up about 10–15% of lung surfactant phospholipids (Hunt et al., 1991; Kahn et al., 1995; Holm et al., 1996). Lung surfactant also contains four apoproteins, including two small hydrophobic proteins (pulmonary surfactant protein SP-B and SP-C) that are known to enhance the adsorption and dynamic film behavior of phospholipids (Hawgood and Schiffer, 1991; Johansson et al., 1994a; Creuwels et al., 1997; Notter, 2000). The lack of surfactant in the under-developed lungs of premature infants is the root cause of respiratory distress syndrome (Avery and Mead, 1959), whereas disruption of surfactant activity is linked to the pathophysiology of clinical lung damage seen in acute respiratory distress syndrome (Pison et al., 1989; Lewis and Jobe, 1993; Notter and Wang, 1997).

Researchers have long used insoluble, monomolecular films spread at the air—water (A/W) interface as models for pulmonary surfactant (Notter, 1984, 2000). Surface balance techniques have been used to study the monolayer properties of the hydrophobic proteins SP-B and SP-C and their mixtures with lipids at the A/W interface (Oosterlaken-Dijksterhuis et al., 1991; Taneva and Keough, 1994a,b,c; Wang et al., 1996). In addition, a variety of biophysical techniques have been used to study surfactant model systems, including electron microscopy (Tchoreloff et al., 1991), Brewster angle microscopy (Discher et al., 1999), fluorescence microscopy (Krüger et al., 1999; Ding et al., 2001; Takamoto et al., 2001), near-field microscopy (Kramer et al., 2000), and scanning probe microscopy (Krol et al., 2000). Although these microscopic techniques provide important biophysical information, they cannot give the same detailed molecular-level information about lipid–protein interactions that can be obtained using vibrational spectroscopic methods.

The use of external reflection Fourier transform infrared spectroscopy (FTIR) to study the structure of monomolecular films directly at the A/W interface was originally developed in the mid 1980s, and progress in this field has recently been reviewed (Mendelsohn et al., 1995; Dluhy, 2000). This infrared reflection-absorption spectroscopy (IRRAS) technique has been applied to the study of monolayer films of extracted lung surfactant preparations (Dluhy et al., 1989) and, more recently, to investigate the roles that SP-B and SP-C play in the function of lung surfactant (Pastrana-Rios et al., 1995; Gericke et al., 1997; Flach et al., 1999). In addition to lipid phase information, it has been shown that amide vibrations can be observed in pure or highly enriched lipid–protein films and that structural information concerning the surfactant proteins can be obtained. Although these

Submitted April 10, 2002 and accepted for publication June 11, 2002.

Address reprint requests to Richard A. Dluhy, Univ. of Georgia, Dept. of Chemistry, Athens, GA 30602-2556. Tel.: 706-542-1950; Fax: 706-542-9454; E-mail: dluhy@chem.uga.edu.

0006-3495/02/10/2126/16 $2.00

studies have contributed significant information to the study of surfactant systems, including the nature of surfactant protein structure and orientation, difficulties remain. In particular, the low band intensities inherent in IRRAS at the A/W interface, and the highly overlapping nature of the amide region makes assignment of protein conformational intermediates problematic.

Recently, an approach using statistical correlation analysis known as two-dimensional infrared spectroscopy (2D IR) has been described to uncover spectral features not readily observable using traditional IR spectroscopy (Noda, 1990, 1993b; Harrington et al., 2000; Noda et al., 2000). Two-dimensional IR spectroscopy is based on the correlation of dynamic spectral variations induced by an external sample perturbation. The effect of these perturbation-induced changes in the local molecular environment is manifested as pseudo time-dependent changes in IR spectral parameters. These resulting dynamic spectra are subject to a cross-correlation analysis that produces 2D maps that can enhance spectral information by spreading out the IR band intensities along two orthogonal axes. 2D IR spectroscopy has particular advantages in simplifying complex spectra, identifying inter- and intramolecular interactions, and facilitating band assignments (Ozaki and Noda, 2000).

Literature references to 2D IR correlation analysis have predominately been in the area of polymer structure, an application for which the method was first developed (Noda et al., 1999). However, the last few years has seen increasing application of this methodology to biological problems, in particular, the use of 2D IR for the study of macroscopic properties of proteins in aqueous solutions. For example, the thermal transitions of a number of proteins has been studied using 2D IR, including cytochrome *c* (Filosa et al., 2001; Paquet et al., 2001), cytosine monophosphate kinases (Schultz et al., 2000), ovalbumin (Wang et al., 1998), β-lactoglobulin (Sefara et al., 1997), avidin (Ismoyo et al., 2000), and synthetic helix-forming peptides (Graff et al., 1997). Several studies have been published that use pH gradients or H–D exchange to enhance the amide spectral region and assign conformations to the underlying band components (Nabet and Pezolet, 1997; Murayama et al., 2001a,b). Studies using 2D hetero-spectral correlations have appeared that enable comparisons to be made among a number of spectral techniques (Kubelka et al., 1999; Pancoska et al., 1999).

Two-dimensional IR correlation analysis has also been used to analyze structure in monomolecular films. The phase behavior of phospholipid monolayers using 2D IR have been studied, and it was shown how these methods could distinguish bands resulting from coexisting phases in a disorder–order phase transition in the monolayer (Elmore and Dluhy, 2000a,b).

Although 2D IR has successfully been used to study structural changes and to make band assignments in proteins, it can also be used in determining the temporal order of events that occur during the external sample perturbation, albeit qualitatively. To more quantitatively describe the degree of coherence between spectral intensity changes and the sequence of molecular events in a set of dynamic spectra, we have recently developed a modified 2D IR correlation method called $\beta\nu$ correlation analysis (Elmore and Dluhy, 2001). This method is a variation of asynchronous cross-correlation, in which dynamically varying spectra are correlated against a mathematical function with varying phase angle. We recently applied $\beta\nu$ correlation analysis to surface pressure-induced changes in the IRRAS spectra of phospholipid monolayers at the A/W interface, and showed how the relative rates of acyl chain and methyl group reorientation could be quantitatively determined (Elmore et al., 2002).

The research described in this paper represents the first study that uses $\beta\nu$ correlation analysis for the study of protein structure. We use this method to probe the conformational intermediates in the surface pressure-resolved IRRAS spectra of two lipid–protein samples: 1,2-dipalmitoyl-*sn*-glycero-3-phosphoglycerol (DPPG)/SP-C and DPPG/SP-B at the A/W interface. Although these proteins have been previously studied using IRRAS at the A/W interface, the detailed study of their conformational intermediates and reorientation in response to increasing surface pressure has not been completely described.

MATERIALS AND METHODS

Surface chemistry

The synthetic phospholipid DPPG was purchased from Avanti Polar Lipids (Alabaster, AL) and was used as received. ACS grade NaCl and HPLC grade methanol and chloroform were obtained from J.T. Baker (Phillipsburg, NJ). Subphase H_2O was obtained from a Barnstead (Dubuque, IA) ROpure/Nanopure reverse osmosis/deionization system having a nominal resistivity of 18.3 MΩ cm.

Purification of SP-B and SP-C

SP-B and SP-C were purified from calf lung surfactant extract (CLSE) by isocratic normal phase liquid chromatography on Silica C8 as described elsewhere (Baatz et al., 2001). Briefly, ~700 mg CLSE (total lipid plus protein) was initially reduced in volume by evaporation under nitrogen to ~4 ml (~1% of column bed volume). Small amounts of chloroform were added to the concentrated CLSE if the solution became cloudy. The concentrated CLSE was then applied to a 450-ml bed volume LC column that had been pre-equilibrated with 7:1:0.4 MeOH/$CHCl_3$/5% 0.1 M HCl. The added CLSE was allowed to completely adsorb to the column, and was then eluted with 7:1:0.4 MeOH/$CHCl_3$/5% 0.1 M HCl at a flow rate of 0.4 ml/min and UV detection at 254 nm. SP-B eluted from the column as the first peak, whereas SP-C eluted as the second peak as determined by SDS PAGE and protein sequencing (see below). SP-B fractions were combined and, as determined by the method of Shin, the final SP-B solution was free of phospholipid (Shin, 1962), whereas SDS PAGE and protein sequencing indicated the absence of SP-C (see below). Fractions containing SP-C were combined, concentrated via N_2 gas stream and run on a second C8 LC column. Fractions containing purified SP-C from this second column were combined. Phospholipid content of purified SP-C using the method of Shin

(1962) was determined to be <4 mole lipid/mole SP-C. Protein sequencing analysis (see below) indicated that the purified SP-C was free of SP-B.

SDS PAGE and amino acid analysis

For SDS PAGE, 20 ml of the appropriate column fractions were suspended in NuPage sample buffer (Invitrogen, Carlsbad, CA) and applied to 4–10% gradient acrylamide Tris/Bis gels (NuPage gels, Invitrogen) under nonreducing conditions. Electrophoresis was performed at a constant voltage of 200 V for 40 min with a morpholinoethanesulphonic acid (MES) buffer containing 50 mM MES/50 mM Tris Base/3.5 mM SDS/1 mM EDTA, pH 7.7 as the running buffer. Silver staining for detection of protein bands was performed according to Morrissey (1981). N-terminal amino acid sequence analysis was performed for seven to ten cycles using an Applied Biosystem Procise sequence analyzer. SP-B and SP-C were identified by the N-terminal sequences of Phe-Pro-Ile-Pro-Ile-Pro and Leu-Ile-Pro-???-???-Pro-Val, respectively, where positions 4 and 5 in the SP-C sequence were both assumed to be Cys. The concentrations of SP-B and SP-C were determined by the BCA total protein assay (Sigma Chemical Co., St. Louis, MO).

Preparation of samples

Stock solutions of DPPG (~2.5 mg/ml in 4:1 $CHCl_3$:MeOH) were prepared and concentrations verified by inorganic phosphorus assay (Chen et al., 1956). Solutions of the lipid and proteins containing 20:1 lipid–protein mol:mol (for SP-C) or 40:1 lipid–protein mol:mol (for SP-B), i.e., ~22 wt% for both SP-B and SP-C, were prepared by mixing the appropriate amounts of the phospholipid stock solution together with the stock solutions of SP-B or SP-C in 1:1 $CHCl_3$:MeOH. The subphase used for all experiments was 150 mM NaCl in deionized H_2O (pH 5.6).

FTIR external reflectance measurements

Infrared external reflection–absorbance spectra of monolayers at the A/W interface were acquired using a Perkin–Elmer Spectrum 2000 FTIR spectrometer equipped with an external sample beam. A 60° gold-coated, off-axis parabolic mirror (Janos Technology Inc., Townshend, VT) reflected the beam coming from the spectrometer onto the surface of a Nima 601M film balance (Coventry, U.K.) at an incidence angle of 30° to the surface normal. The beam reflects off of the subphase, sampling the film, and a second parabolic mirror collects the beam and directs it into a collection mirror and then onto the sensing chip of a liquid N_2-cooled HgCdTe detector. The film balance, optical components, and detector are housed in a sealed, Plexiglas chamber that allows humidity control of the local trough environment, thus improving water vapor background subtraction. A schematic diagram of the experimental set-up has been previously published (Dluhy, 2000).

The subphase was first cleaned by aspiration, and a single beam spectrum was collected for use as the IR background spectrum. The subphase temperature was held constant at 22 ± 1°C by flowing thermostatted water through the hollow body of the trough. The temperature in the enclosed chamber was typically 24°C and the relative humidity remained fairly constant at 70%. Typically 5–10 μl of sample was spread via syringe onto the trough surface. The film was allowed to equilibrate for a period of 30 min and then was compressed intermittently and spectra collected over a range of surface pressures from ~5 mN/m to a maximum of 45–65 mN/m depending on the nature of the film.

External reflection–absorption spectra were collected with 1024 scans at 16-cm^{-1} resolution, apodized with a Norton–Beer (medium) function, and were Fourier transformed with one level of zero filling. A resolution of 16 cm^{-1} was chosen for several reasons: 1) time of collection is minimized and SNR is maximized when spectra are collected at lower resolution, 2) residual water vapor bands are easier to subtract at low resolution when the relative humidity varies slightly during the course of the experiment, and 3) valid statistical correlation analyses can be constructed for IR spectra collected at lower resolutions, as has recently been discussed (Berry and Ozaki, 2001).

All monolayer spectra are presented as reflection–absorption spectra, i.e., $A = -\log(R/R_0)$, where R is the IR reflectivity of the monolayer surface and R_0 is the IR reflectivity of the bare water subphase background. The reflectance IR spectra used in the analyses presented here were baseline corrected using the GRAMS/32 (Galactic Industries, Salem, NH) software package before determination of peak positions and band intensities; in addition, residual water vapor bands have been subtracted. Adjustments for changes in surface density (i.e., intensity normalization) were also performed using GRAMS/32. Other than baseline correction and intensity normalization, the spectra have not been smoothed or further processed. Vibrational frequencies were calculated using a 5-point center of gravity algorithm (Cameron et al., 1982) written in our laboratory for the Grams/32 environment.

Calculation of 2D IR correlation spectra

The 2D IR synchronous spectrum, $\Phi(\nu_1, \nu_2)$, and the asynchronous spectrum, $\Psi(\nu_1, \nu_2)$, were calculated using Eqs. 1 and 2. These algorithms use the most recent mathematical formalism in which a Hilbert transform is utilized for calculating the asynchronous spectrum rather than the more commonly used Fourier transform (Noda, 2000). In all cases, the average spectrum was subtracted from each sequentially obtained surface pressure-dependent IRRAS spectrum to produce a set of dynamic IR spectra. The dynamic spectra were then used in the correlation analysis

$$\Phi(\nu_1, \nu_2) = \frac{1}{N-1}\sum_{j=0}^{N-1} y(\nu_1, n_j)\cdot y(\nu_2, n_j) \qquad (1)$$

$$\Psi(\nu_1, \nu_2) = \frac{1}{N-1}\sum_{j=0}^{N-1} y(\nu_1, n_j)\cdot \sum_{k=0}^{N-1} M_{jk}\cdot y(\nu_2, n_k). \qquad (2)$$

In Eqs. 1 and 2, ν_1 and ν_2 represent two independent frequencies, n_j represents the number of the spectrum in the ordered sequence where the first spectrum number is zero, N represents the total number of spectra used in the calculation, and M_{jk} is the Hilbert transform matrix, which is defined in

$$M_{jk} = \begin{cases} 0 & \text{if } \; j = k \\ 1/\pi(k-j) & \text{otherwise} \end{cases} \cdot \qquad (3)$$

The 2D plots presented in this article were calculated using 2D IR correlation analysis algorithms written in our laboratory for the METLAB programming environment (Version 6, The MathWorks, Inc., Natick, MA).

$\beta\nu$ Correlation analysis

A $\beta\nu$ correlation analysis is a mathematical asynchronous cross correlation performed on a set of dynamically varying IR spectra against a set of sinusoidal functions that differ only by their phase angle β. A full description of the details of the $\beta\nu$ correlation analysis has been presented elsewhere (Elmore and Dluhy, 2001). This type of correlation analysis is mathematically described using

$$\Psi(\nu, \beta) = \frac{1}{N-1}\sum_{j=0}^{N-1} y(\nu, n_j)\cdot \sum_{k=0}^{N-1} M_{jk}\cdot \sin(k\phi + \beta). \qquad (4)$$

The correlation intensity Ψ at some point (ν, β) represents the correlation of the measured IR spectral intensity $y(\nu, n_j)$ with the mathematical function $\sin(k\phi + \beta)$. In Eq. 4, y is the IR intensity; ν is the frequency or wavenumber; n_j is the number of the spectrum in the ordered sequence where the first spectrum number is zero; β is the phase angle of the respective sine function; N is the total number of spectra used in the calculation; ϕ is a constant value in degrees (or radians) chosen based upon the total number of dynamic spectra used in the calculation, and M_{jk} is the Hilbert transform matrix previously defined in Eq. 3.

In this study, all $\beta\nu$ correlations were performed with $\phi = 10^o$, so that $\sin(k10° + \beta)$ describes ~¼ of the cycle of a sine function, or the approximate form of a commonly observed variation in spectral band intensities upon sample perturbation. Only the asynchronous correlation algorithm is used in the $\beta\nu$ correlation analysis presented here, since asynchronous 2D IR correlations are more sensitive to differences in the form of the signal variation than are synchronous correlations (Noda, 1990). Note also that the computational algorithm for the $\beta\nu$ correlation analysis uses the most recent mathematical formalism, in which a Hilbert transform is used for calculating the asynchronous spectrum, rather than the more computationally cumbersome Fourier transform (Noda, 2000).

The effective phase angle, β_e, is defined by

$$\beta_e = \beta + 90°. \quad (5)$$

In Eq. 5, β is the point of maximum positive correlation intensity in the plot of β versus ν as defined by Eq. 4. The value of β_e is defined in this fashion so that the phase angle β and the effective phase angle β_e are the same for a sinusoidal signal variation with constant frequency. In this article, the contour levels are evenly spaced in the $\beta\nu$ plots from 0 to the maximum value for positive correlations. Negative correlations are not displayed because they simply differ from the positive correlations by 180^o. The $\beta\nu$ plots of effective phase angles versus wavenumber were calculated using $\beta\nu$ correlation analysis algorithms written in our laboratory for the MATLAB programming environment.

RESULTS AND DISCUSSION

IRRAS spectra of lipid:protein monolayer films

Infrared external reflectance–absorption spectra were obtained at the A/W interface for monolayer films of DPPG plus the surfactant proteins SP-B and SP-C. These spectra are shown in Fig. 1. These IR spectra were acquired while the monolayer was held at specific surface pressure values from 4.0 mN/m to 40.0 mN/m during step-wise compression of the film balance. External reflection–absorption IR spectra of monomolecular films at the A/W interface differ substantially from spectra obtained by conventional transmission IR spectroscopy. In particular, the complex refractive indices of both sample and substrate contribute to the observed IRRAS spectra of A/W monolayers. Therefore, these spectra are functions of the wavelength, state of polarization, thin film thickness, angle of incidence of the incoming light, and the optical constants of the three phases involved (Dluhy, 1986). The physical basis for the method and the use of IR spectroscopy to study monolayer films at the A/W interface has recently been reviewed (Mendelsohn et al., 1995; Dluhy, 2000).

Monolayer IRRAS spectra were collected using an unpolarized incident IR source and have been normalized to account for changes in trough area. Normalization refers to

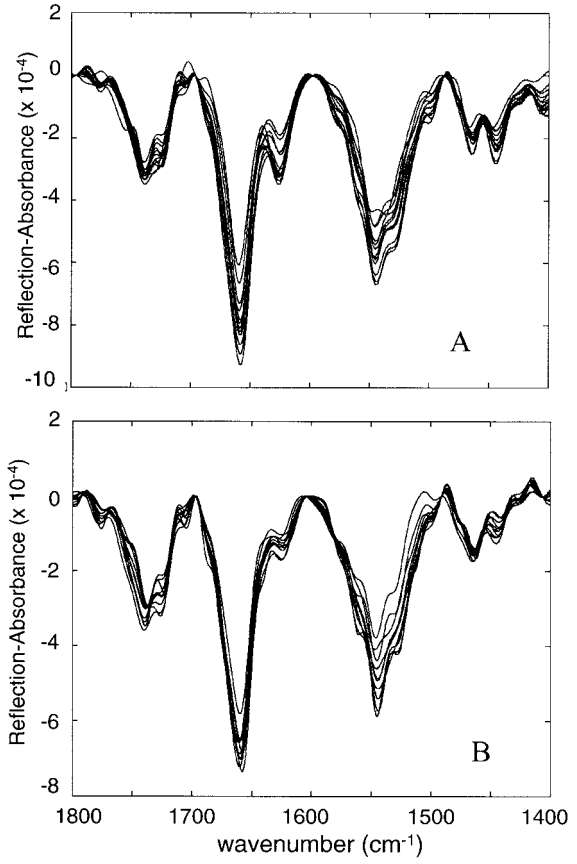

FIGURE 1 IR external reflection–absorption spectra of a lipid:protein monolayer showing the amide I and amide II spectral regions collected at surface pressures from 4.0 to 40.0 mN/m. The spectra were collected as a function of increasing monolayer surface pressure and have been normalized for changes in surface density. (*A*) DPPG/SP-C (20:1, mol:mol, ~22 wt% SP-C). (*B*) DPPG/SP-B (40:1 mol:mol, ~22 wt% SP-B).

the adjustment of IR spectral intensities to take into account changes in surface density as the trough area available to the monomolecular film decreases during compression. Intensity changes in area-normalized monolayer spectra more accurately reflect conformational changes in the monolayer, as opposed to merely reflecting an increase in number density. We have previously shown that intensity normalization is important for understanding 2D IR correlation maps calculated from IRRAS monolayer spectra (Elmore and Dluhy, 2000b). In addition, the spectra used in these analyses were collected at 16-cm^{-1} resolution. The issue of resolution is particularly relevant to monolayer IRRAS at the A/W interface, because it is a low-intensity reflectance technique with inherently weak (10^{-3}–10^{-4} AU) band intensities. Due to the very broad amide I proteins bands (bandwidths > 30 cm^{-1}), a spectral resolution of 16 cm^{-1} was used to minimize collection time and maximize signal to noise. A recently published paper has addressed instrumental issues in the calculation of 2D IR spectra and has shown that lower resolution spectra may be appropriate for

use in 2D calculations under certain circumstances (Berry and Ozaki, 2001).

The overlaid spectra in Fig. 1 are reflection–absorbance spectra displaying the amide I (1700–1600 cm^{-1}) and amide II (1600–1500 cm^{-1}) regions of the surfactant proteins. Also observed is the C═O vibration from the phospholipid between 1750 and 1700 cm^{-1}. These IRRAS absorption bands exhibit negative IR intensities, in agreement with the experimental conditions (Dluhy, 1986). Figure 1 *A* illustrates IRRAS spectra at the A/W interface for a DPPG/SP-C monolayer at a protein concentration of ~22 wt%. Clearly evident in the spectra are the lipid C═O band at 1738 cm^{-1}, two protein amide I bands at ~1654 and 1625 cm^{-1}, and the protein amide II band at ~1550 cm^{-1}. Figure 1 *B* illustrates the same spectral regions as in Fig. 1 *A* for a DPPG/SP-B monolayer also at a protein concentration of ~22 wt%. The identical carbonyl and amide bands are evident in the spectra of the SP-B monolayer as in the spectra of the SP-C monolayer, although relative band heights for the amide vibrations differ.

Identification of unique surface pressure regimes using windowed autocorrelation analysis

Before analysis of the lipid–protein monolayer spectra using 2D IR correlation spectroscopy, we used a windowed autocorrelation method to identify the surface pressure regimes that encompass the greatest variation in amide spectral intensity. These regions can be located by adapting a dynamic filtering technique that autocorrelates IR intensities within a defined surface pressure window and plots them against the average surface pressure, thereby locating the regions of maximal spectral variation. This technique has been previously applied to the temperature-dependent 2D IR spectra of liquid crystals (Thomas and Richardson, 2000).

The windowed autocorrelation analysis method begins by separating the monolayer IRRAS spectra into a smaller data set containing only the first four spectra of lowest surface pressure (e.g., P_1 through P_4). An average spectrum is calculated from the spectra in this window; the individual spectra in the window are mean-centered by subtraction of the average. Next, 2D IR analysis is used to calculate the correlation intensities for each spectral frequency in this windowed, mean-centered data set. The resulting autocorrelation intensities represent the amount of spectral variation that occurs at each frequency as a function of the average surface pressure of the windowed data set. This autocorrelation window is then swept over the entire data set, translating it one surface pressure-resolved spectrum at a time (i.e., the second window contains P_2 through P_5, etc.).

The autocorrelation spectrum that results from this process is plotted as a function of the average surface pressure of the autocorrelation window. The spectral frequencies that have the largest autocorrelation intensities will be those frequencies at which the largest spectral variations occur. In this manner, surface pressure regions that contain maximal spectral variations may be identified. With this information at hand, 2D IR or $\beta\nu$ correlation analysis can be performed solely within these regions to establish the structural or temporal relationships that contribute to the spectral variations.

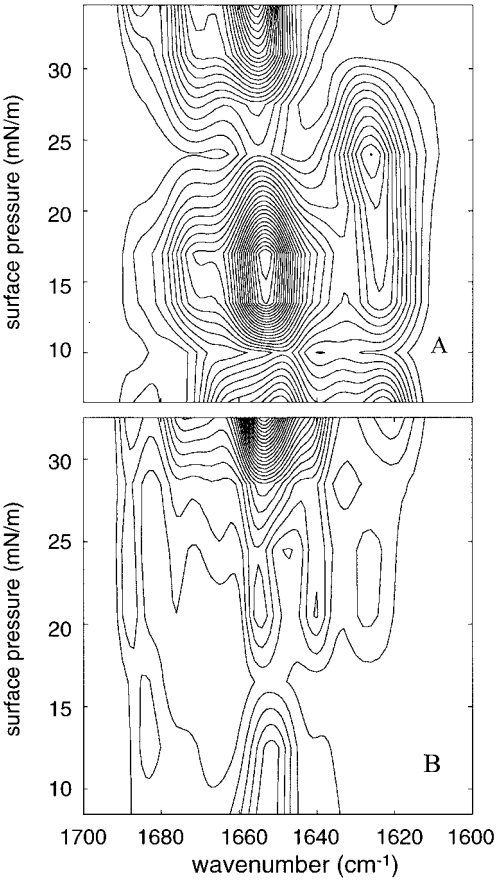

FIGURE 2 Surface pressure–wavenumber contour plot of autocorrelation intensities based on a dynamic filtering technique using a windowed autocorrelation analysis method. Contours result from the autocorrelation intensities calculated as a function of a translating surface pressure window. (*A*) DPPG/SP-C (20:1, mol:mol, ~22 wt% SP-C). (*B*) DPPG/SP-B (40:1 mol:mol, ~22 wt% SP-B).

We have applied this windowed autocorrelation analysis method to the monolayer IRRAS spectra of DPPG/SP-C and DPPG/SP-B. The results are shown in Fig. 2. In analyzing these spectra, we were particularly concerned with the protein structural components, hence we concentrated on autocorrelation of the amide I spectral region. Figure 2 *A* shows a contour plot of the autocorrelation spectra for the DPPG/SP-C sample. This contour plot is dominated by a large band at ~1650 cm^{-1} that shows two intensity maxima: one between ~12 and 18 mN/m and one above ~27 mN/m. Based on these autocorrelation spectra, we can reliably partition the surface pressure-resolved spectra of the

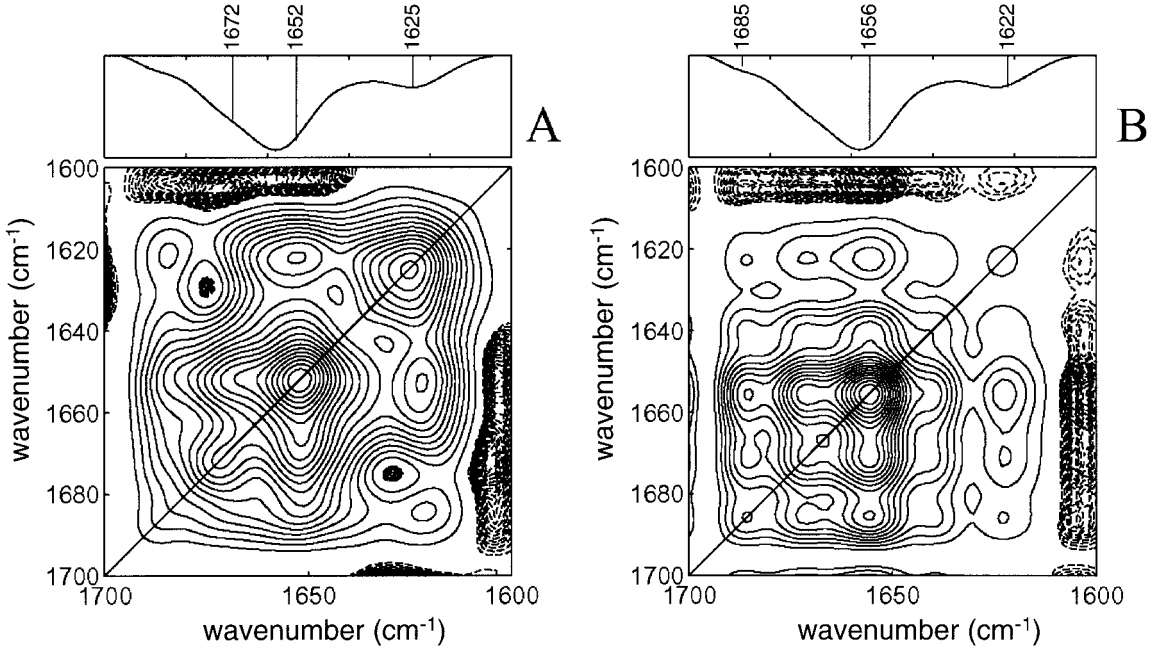

FIGURE 3 Synchronous 2D IR correlation plots of the monolayer IRRAS spectra of DPPG/SP-C (20:1, mol:mol, ~22 wt% SP-C). Solid lines indicate regions of positive correlation intensity; dashed lines indicate regions of negative correlation intensity. Spectra were divided into two pressure regions based on their autocorrelation intensities. 2D IR synchronous correlations were calculated on spectra contained within the pressure region. The one-dimensional spectrum shown in this figure is the calculated average of the spectra used in the 2D analysis. (*A*) 4.0–25.0 mN/m. (*B*) 25.0–40.0 mN/m.

DPPG/SP-C monolayer into two pressure regions, low (4–25 mN/m) and high (25–40 mN/m). A similar contour plot of the autocorrelation intensities for the DPPG/SP-B spectra is shown in Fig. 2 *B*. In this case, an intense autocorrelation maxima at ~1650 cm^{-1} is observed at high surface pressure (25 mN/m), however, lower intensity contours occur below 25 mN/m. Therefore, we have also divided the surface pressure-resolved spectra of the DPPG/SP-B monolayer into two pressure regimes: low (4–25 mN/m) and high (25–40 mN/m). The approach that we have taken here isolates the surface pressure regions that contain maximal spectral variations. Using these newly defined surface pressure regimes, we have performed 2D IR and $\beta\nu$ correlation analyses on the IRRAS spectra of both the SP-C- and SP-B-containing monolayers to better understand the surface pressure-induced protein rearrangements in the monolayer.

2D IR correlation analysis of the SP-C amide I region

Synchronous and asynchronous 2D IR correlation maps were calculated for the SP-C-containing monolayer to investigate protein conformational changes that occur upon monolayer compression. Figure 3 shows the 2D contour map for the synchronous correlation of the DPPG/SP-C IRRAS spectra, in both the low surface pressure regime below 25 mN/m (Fig. 3 *A*) and the high surface pressure region above 25 mN/m (Fig. 3 *B*). Synchronous 2D spectra are characterized by on-diagonal auto peaks and off-diagonal, symmetric cross-peaks. Synchronous 2D auto peaks simply reflect how the spectral intensity responds to the external perturbation; synchronous cross-peaks, in contrast, develop when two separate transition dipole moments are significantly coupled, or if they reorient in phase to the external perturbation (Noda, 1993a).

Note that, due to the symmetric properties of synchronous correlation cross-peaks with respect to the diagonal, it is necessary to describe only the cross-peaks above the diagonal line. This property also holds for the antisymmetric properties of the cross-peaks in the asynchronous correlation plots (see below). In this article, correlation peaks are described as ν_1 versus ν_2, where ν_1 refers to the wavenumber value of the *x* axis and ν_2 refers to the wavenumber value of the *y*-axis.

Mature SP-C consists of 35 amino acids and is an extremely hydrophobic, predominately α-helical protein of approximately 4.2 kD with charged amino acids (K10 and R11) near its N terminus. The cysteines C4 and C5 are acylated in bovine SP-C. The NMR structure of SP-C in apolar solvent essentially describes the protein as a rigid rod in which only a few residues near the N terminus (L1–P7) and the C terminus itself are not helical (Johansson et al., 1994b). The length of this helix (V8–G34) is ~39 Å with a diameter of ~12 Å.

The 2D IR synchronous map of the low-pressure region of the DPPG/SP-C monolayer (Fig. 3 *A*) is dominated by a strong auto peak at 1652 cm^{-1} with less intense auto peaks at 1672 and 1625 cm^{-1}. Positive cross-peaks are observed at 1652 versus 1625 cm^{-1} and 1685 versus 1625 cm^{-1}. Positive synchronous cross-peaks indicate a coordinated spectral response in which the functional groups are reorienting in the same direction. In addition, there is a negative cross-peak between the 1676 versus 1630 cm^{-1} bands. Negative synchronous cross-peaks also indicate significantly coupled molecular reorientation, albeit one where the spectral intensity of one component increases while the second decreases.

The high surface pressure region (>25 mN/m) of the DPPG/SP-C monolayer is also dominated by the major auto peak at 1656 cm^{-1} (Fig. 3 *B*) with additional auto peaks observable at 1685, 1671, 1666, and 1622 cm^{-1}. Cross-peaks associated with the 1622-cm^{-1} band can be observed at wavenumber values 1656 versus 1622 cm^{-1}, 1671 versus 1622 cm^{-1} and 1685 versus 1622 cm^{-1}. Additional cross-peaks at 1671 versus 1654 cm^{-1} and 1685 versus 1654 cm^{-1} are also observed.

The wavenumber location of the cross-peaks in the 2D IR synchronous map can be identified with protein secondary structure conformations (e.g., α-helices, β-sheets, and turns, unordered structure, etc.) using previously published IR correlations, see e.g., Byler and Susi (1986), Surewicz et al. (1993), Goormaghtigh et al. (1994), and Jackson and Mantsch (1995). Caution is advisable when making conformational assignments using IR amide I spectra because secondary structure correlations with a specific wavenumber are not unique, and a wavenumber range exists in the amide I region for any particular protein conformation. Nevertheless, using the most well-established associations, the cross-peak at 1654 cm^{-1} can be considered characteristic of α-helices, whereas the bands at 1630 and 1676 cm^{-1} are assigned to β-sheet and β-turn/loop structures, respectively.

In both the raw spectra (Fig. 1) and the synchronous and asynchronous (see below) 2D maps for DPPG/SP-C, we also observe bands and cross-peaks at wavenumber values both high (1687 cm^{-1}) and low (1620 cm^{-1}) in the amide I range. Using ab initio calculations, this pair of peaks has been assigned to a structure of extended, multistranded, antiparallel β-sheet aggregates (Kubelka and Keiderling, 2001); these peaks have also been experimentally observed for a model β -sheet peptide (Khurana and Fink, 2000). This association is strengthened in the case of SP-C, because the 2D synchronous maps for both low and high pressures show a cross-peak between 1687 and 1620 cm^{-1}, indicating a coordinated response between the two bands. The implication for SP-C, a predominately α-helical protein (Johansson et al., 1994b), is that some portion of the molecule undergoes intermolecular hydrogen bonding resulting from aggregation of unfolded protein segments.

Taking these structural assignments into account, the synchronous 2D map for SP-C shows that the α-helix is the predominate structural motif in both the low and high pressure regions, as expected. However, the cross-peaks at 1625, 1630, 1672, and 1685 cm^{-1} also demonstrate that SP-C contains a more varied secondary structure containing a higher degree of aggregated β-strands than previously reported.

Asynchronous 2D IR correlation maps were also calculated from the DPPG/SP-C IRRAS monolayer spectra. In a similar fashion to the synchronous plots of Fig. 3, Fig. 4 shows the 2D contour map for the asynchronous correlation of the DPPG/SP-C spectra, in both the low surface pressure regime below 25 mN/m (Fig. 4 *A*) and the high surface pressure region above 25 mN/m (Fig. 4 *B*). Asynchronous 2D spectra are antisymmetric with respect to the diagonal in the correlation map and contain no auto peaks; the spectrum consists only of off-diagonal cross-peaks with two intensity maxima—one positive and one negative. Peaks appear in asynchronous 2D correlation maps if the transition dipole moments are significantly decoupled, or if the dipole moments reorient out-of-phase or at different rates in response to the external perturbation. This attribute is used to unmask the differential response of functional groups in the molecule, and makes asynchronous 2D correlation plots particularly useful for resolution enhancement (Noda, 1993a).

The asynchronous 2D IR map of SP-C also indicates the presence of a varied, heterogeneous secondary structure for SP-C, in agreement with the synchronous correlation spectra. Four prominent cross-peaks are observed in the low-pressure region (Fig. 4 *A*) at 1652 versus 1634 cm^{-1} (−), 1663 versus 1652 cm^{-1} (+), 1675 versus 1663 cm^{-1} (−) and 1685 versus 1675 cm^{-1} (+). Less intense, broad cross-peaks are observed for the association of the band attributed to a β-sheet intermolecular aggregation (~1615 cm^{-1}) with the bands 1634, 1652, and 1663 cm^{-1}. The presence of asynchronous cross-peaks at 1615, 1634, 1675, and 1685 cm^{-1} confirms the presence of these bands in the synchronous spectrum, and indicates that the SP-C protein conformation is composed of extended β-sheet structure.

In the high pressure region above 25 mN/m, the asynchronous 2D correlation plot for DPPG/SP-C is characterized by a number of different cross-peaks (Fig. 4 *B*), with a more complicated cross-peak structure than is observed in the asynchronous spectrum of the low-pressure region. Major positive asynchronous correlations are observed between 1654 versus 1647 cm^{-1}, 1675 versus 1647 and 1665 cm^{-1}, with an elongated correlation intensity band at 1688 versus 1647, 1665 and 1680 cm^{-1}. Major negative asynchronous correlations are observed between 1665 versus 1654 cm^{-1} and 1680 versus 1654 and 1675 cm^{-1}. In addition, there is an elongated negative correlation intensity band between ~1647–1680 versus 1625 cm^{-1}.

The most relevant features of the asynchronous spectrum for the high pressure region are the split α-helix peak at 1654/1647 cm^{-1}, the elongated correlation intensity max-

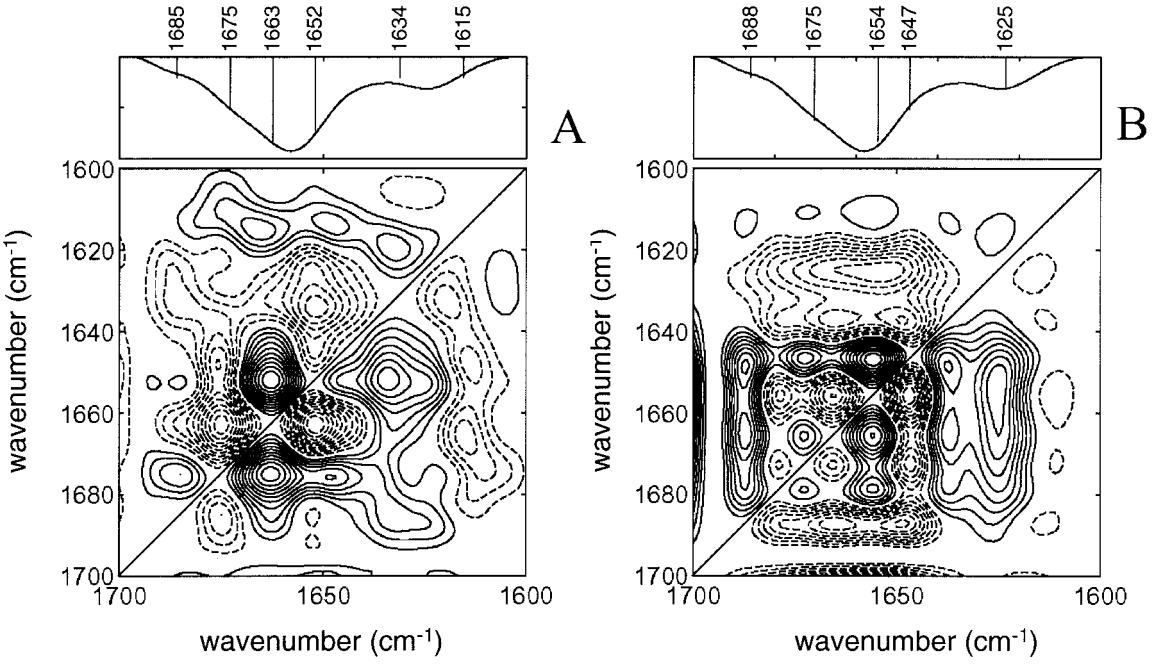

FIGURE 4 Asynchronous 2D IR correlation plots of the monolayer IRRAS spectra of DPPG/SP-C (20:1, mol:mol, ~22 wt% SP-C). Solid lines indicate regions of positive correlation intensity; dashed lines indicate regions of negative correlation intensity. Spectra were divided into two pressure regions based on their autocorrelation intensities. 2D IR asynchronous correlations were calculated on spectra contained within the pressure region. The one-dimensional spectrum shown in this figure is the calculated average of the spectra used in the 2D analysis. (*A*) 4.0–25.0 mN/m. (*B*) 25.0–40.0 mN/m.

ima associated with the 1680 cm^{-1} band, and the elongated correlation intensity minima associated with the 1625 cm^{-1} band. The ability of asynchronous 2D IR to resolve overlapped peaks is demonstrated in Fig. 4 *B* because the low-pressure asynchronous α-helix cross-peak at 1652 cm^{-1} has divided into two components at high pressure, one at 1654 cm^{-1} and one at 1647 cm^{-1}. This is the first report of two coexisting α-helix conformations in SP-C lipid–protein monolayers at high surface pressure. The 1647-cm^{-1} helix band, in particular, shows asynchronous cross-peaks with a number of other bands, including 1654, 1675, and 1680 cm^{-1}, indicating an out-of-phase response of this conformation with the other protein conformations. These large elongated asynchronous correlation features at 1620 and 1680 cm^{-1} indicate that the motion of the extended β-structure is also significantly decoupled from the rest of the protein and reorients independently of the main helix structure at high surface pressures.

The asynchronous correlation spectrum for SP-C (Fig. 4) presents a more complex band structure than does the synchronous correlation spectrum (Fig. 3). The multiple cross-peaks observed in the asynchronous correlation plot demonstrate that SP-C is composed of a varied secondary structure. The major result of the asynchronous 2D correlation analysis is that the main α-helix band splits into two peaks at high surface pressures, indicating two different coexisting helix conformations for SP-C. The peaks at ~1634 and 1675 cm^{-1} indicate that a β-sheet structure exists at both low and high surface pressures. Also, the cross-peaks at ~1620 and 1680 cm^{-1} demonstrate that an intermolecular aggregation of extended β-sheet structure exists in the monolayer. This is possibly due to the relatively high amount of SP-C in the monolayer (~22 wt%), as compared to the physiologically relevant concentration of ~1 wt%. A previous IRRAS study has documented the presence of protein aggregation in highly enriched lipid/SP-C monolayers (Pastrana-Rios et al., 1995). However, other more recent research suggests that monomeric α-helical SP-C is thermodynamically metastable, with the peptide irreversibly forming β-sheet aggregates resembling amyloid fibrils, which may be implicated in pulmonary alveolar proteinosis (Szyperski et al., 1998; Gustafsson et al., 1999). Therefore, the presence of several α-helix conformations and the β-aggregate bands in the 2D spectra may indicate an intermediate in the α-to-β conversion, which is known to be a slow, kinetically controlled process. This is the first time that specific IR evidence has demonstrated that multiple α-helix conformations and β-structure conformational intermediates exist for SP-C-containing monolayers at the A/W interface.

$\beta\nu$ Correlation analysis of the SP-C amide I region

In addition to its use in studying structural changes and making band assignments, 2D IR correlation spectroscopy

has also been used to determine the temporal order of events that occur during the external sample perturbation. The basis for this determination is the relative signs of the asynchronous and synchronous cross-peaks (Noda, 1993a). A positive asynchronous cross-peak at (ν_1, ν_2) indicates that the intensity change at ν_1 occurs before ν_2; A negative cross-peak at ν_1 is observed if the change occurs after ν_2. This rule, however, is reversed if the corresponding synchronous peak at (ν_1, ν_2) has a negative sign, i.e., $\Phi(\nu_1, \nu_2) < 0$. Although it is possible to determine the relative sequence of molecular rearrangements based on comparison of the signs of the cross-peaks in the asynchronous versus synchronous correlation maps, this procedure is somewhat cumbersome, inherently qualitative in nature, and leads to uncertainties for highly overlapped spectra.

To more quantitatively describe the degree of coherence between the observed spectral intensity changes and the sequence of molecular events in a discrete set of dynamic spectra, we have recently developed a modified 2D IR correlation method called $\beta\nu$ correlation analysis (Elmore and Dluhy, 2001). In this method an asynchronous cross-correlation is performed using a set of dynamically varying spectra, i.e., $y(\nu, n_j)$, against a mathematical function that approximates the functional form that the external perturbation induces on the IR spectral intensities. To date, we have used a sine function, e.g.,. $\sin(k\phi + \beta)$. The resulting correlation intensities are a function of the spectral frequency (ν) and the phase angle (β) of the mathematical function. The maximum correlation intensity will be observed at one point (ν, β) in the correlation plot for the range $360 > \beta > 0$; this point is used to define a new parameter—the effective phase angle β_e of $f(\nu, \beta)$. The β_e value quantitatively reveals the degree of coherence between the experimental intensities and the sequence of molecular events in a discrete set of dynamic spectra. We recently applied $\beta\nu$ correlation analysis to surface pressure-induced changes in the IRRAS spectra of phospholipid monolayers at the A/W interface, and showed how the relative rates of acyl-chain and methyl-group reorientation could be quantitatively determined (Elmore et al., 2002).

The $\beta\nu$ correlation plot for the amide I region of SP-C at low surface pressure (<25 mN/m) is shown in Fig. 5 *A*. In addition, the values for the effective phase angle (β_e) and the band assignments for the peaks in this plot are presented in Table 1. It is immediately obvious from Fig. 5 *A* that the most intense peak in the $\beta\nu$ plot is observed at 1650 cm^{-1} and corresponds to the α-helix of SP-C. However, peaks due to β strands (1663 cm^{-1}) and to extended, aggregated β structures (1620 and 1682 cm^{-1}) are also apparent. (The peak at 1606 cm^{-1} is likely due to a side-chain vibration and is not included in this analysis.) It is also apparent from Fig. 5 *A* and Table 1 that each of the amide I peaks for SP-C at low surface pressures have nearly identical β_e values, with a standard error of <1% relative to the mean. These data confirm that all segments of the SP-C protein reorient at the identical relative rate when the surface pressure is increased up to 25 mN/m.

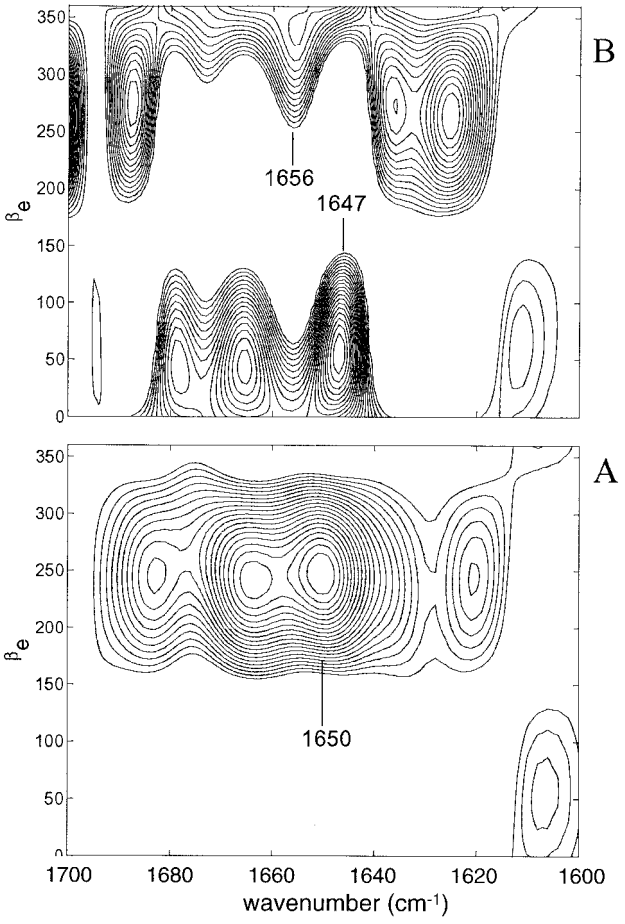

FIGURE 5 $\beta\nu$ Correlation plots derived from the monolayer IRRAS spectra of DPPG/SP-C (20:1, mol:mol, ~22 wt% SP-C). Spectra were divided into two pressure regions based on their autocorrelation intensities. $\beta\nu$ correlations were calculated on spectra contained within the pressure region. (*A*) 4.0–25.0 mN/m. (*B*) 25.0–40.0 mN/m.

The relative reorientation of SP-C secondary structure becomes more complicated at high surface pressures (25–40 mN/m), as illustrated in Fig. 5 *B*. As seen in Table 1, the β_e values at high pressures divide into three identifiable groups. The largest effective phase angle (indicative of the most rapid reorientation) is that of the 1656 cm^{-1} peak with $\beta_e = 341.9$, attributable to the high wavenumber α-helix conformation. The second group to reorient includes the peaks at 1687 cm^{-1} ($\beta_e = 273.4$), 1636 cm^{-1} ($\beta_e = 270.9$), and 1625 cm^{-1} ($\beta_e = 263.5$), all of which can be attributed to extended β-sheet structures. Last, the third group to reorient at a much slower relative rate includes the peaks at 1678 cm^{-1} ($\beta_e = 40.5$), 1665 cm^{-1} ($\beta_e = 43.0$), and 1647 cm^{-1} ($\beta_e = 53.2$). The cross-peaks in this group are associated with β turn/loop structures and the low wavenumber α-helix conformation. The $\beta\nu$ plot at high surface pressures (Fig. 5 *B*) shows that most of the correlation

TABLE 1 Effective phase angle, β_e, values calculated for DPPG/SP-C monolayer IRRAS spectra in amide I region

Wavenumber (cm^{-1})	β_e Value	Assignment
Region A:	4.0–25.0 mN/m	
1682.8	244.8	β strand (aggregated)
1663.4	243.5	β turn/loop
1650.2	247.3	α helix
1620.4	244.8	β strands (aggregated)
1606.3	54.2	Side chain
Region B:	25.0–40.0 mN/m	
1687.4	273.4	β strand (aggregated)
1678.3	40.5	β turn/loop
1665.4	43.0	β turn/loop
1655.9	341.9	α helix
1647.1	53.2	α helix
1636.0	270.9	β sheet
1625.1	263.5	β strand (aggregated)
1611.0	60.4	Side chain

β_e Values taken from the $\beta\nu$ 2D correlation plots for the DPPG/SP-C monolayer (Figure 5).

intensity of the two α-helix peaks is concentrated in the lower wavenumber peak at 1647 cm^{-1}, which is also the helix conformation that reorients the slowest.

A consideration of the 2D IR and β_e values for SP-C leads to the following model for protein reorientation. At low surface pressures, the protein exists in a variety of secondary structure conformations, most noticeably the predominate α-helix, but also including extended β-sheet structures. All conformations of the SP-C molecule react identically to increasing surface pressure and reorient in phase with each other. Above 25 mN/m, however, the increasing surface pressure selectively affects the coexisting protein conformations and leads to an independent reorientation of these protein subunits. The high wavenumber α-helix conformation reorients first, closely followed by the reorientation of the extended β structures, including that of the aggregated protein strands. The last protein reorientational motion to occur originates from the low-wavenumber α-helix conformation and from β turn/loop and unordered structures, which are most likely due to very short protein fragments that link together the more ordered protein segments. The reorientation motion of this second helix conformation and the β turn/loop fragments lags significantly behind the reorientation rates of the other ordered (α and β) protein segments. As the majority of the $\beta\nu$ correlation intensity is concentrated in this second helix conformation, it is presumably this conformation that orients its helix axis toward the surface normal, as previously described (Gericke et al., 1997).

It is possible that the selective reorientation of the two α-helix conformations plays a role in the SP-C-mediated formation of three-dimensional, surface-associated, lipid–protein structures at high surface pressures. Using microscopic techniques methods, these structures have been observed to be formed at high surface pressures when human recombinant or synthetic SP-C is incorporated in lipid monolayers (Galla et al., 1998; Bourdos et al., 2000; Kramer et al., 2000). Although models have been proposed for the formation of these structures, the details of how SP-C facilitates their development is still unknown. However, reorientation of the α-helix is postulated to play a pivotal role.

2D IR correlation analysis of the SP-B amide I region

We have also used 2D correlation methods to study protein conformational changes in monolayers of DPPG/SP-B. In contrast to the DPPG/SP-C monolayers, the DPPG/SP-B samples were prepared at a 40:1 ratio (lipid:protein, mol:mol). Due to the higher molecular weight of SP-B, however, this mol ratio still equates to ~22 wt% protein in the monolayer. As described above, we have used a windowed autocorrelation method to divide the DPPG/SP-B monolayer spectra into two separate regions for detailed analysis (Fig. 2 *B*). The autocorrelation method defines a low-pressure regime (4–25 mN/m) and a high pressure regime (25–40 mN/m) for DPPG/SP-B monolayers, similar to the case of DPPG/SP-C.

The mature form of SP-B is a highly charged protein containing 79 amino acids of ~18 kD. A high percentage of these amino acids are cysteine, basic, or hydrophobic residues. The protein exists as a disulfide-linked homodimer (Hawgood et al., 1987) and is expected to have several amphipathic α-helical segments on both the amino and carboxy terminal ends (Gustafsson et al., 1999). In addition, each SP-B monomer contains three intramolecular disulfide bridges linking cysteines residues; a fourth disulfide bridge is responsible for the intermolecular dimerization. Evidence suggests that SP-B is not a transmembrane or transmonolayer protein. IR results of lipid–protein vesicles (Vandenbussche et al., 1992) demonstrated that domains of SP-B are associated with the phospholipid headgroups, whereas other domains are located inside the bilayer. Fluorescence anisotropy also determined that SP-B was not a transmembrane protein, but was associated with the membrane surface (Baatz et al., 1990). The polypeptide motif of the SP-B monomer is characterized by amphiphatic α-helices with solvent-associated hydrophilic side chains, whereas other hydrophobic conformations form a protein core stabilized by intramolecular disulfide bonds (Hawgood et al., 1998).

Figure 6 shows the 2D contour map for the synchronous correlation of the DPPG/SP-B IRRAS spectra, in both the low surface pressure regime below 25 mN/m (Fig. 6 *A*) and the high surface pressure region above 25 mN/m (Fig. 6 *B*). The synchronous map of the low-pressure region (Fig. 6 *A*) is dominated by strong auto peaks at 1653 and 1686 cm^{-1} with less intense auto peaks at 1640 and 1625 cm^{-1}. Positive cross-peaks are formed between the α-helix band at

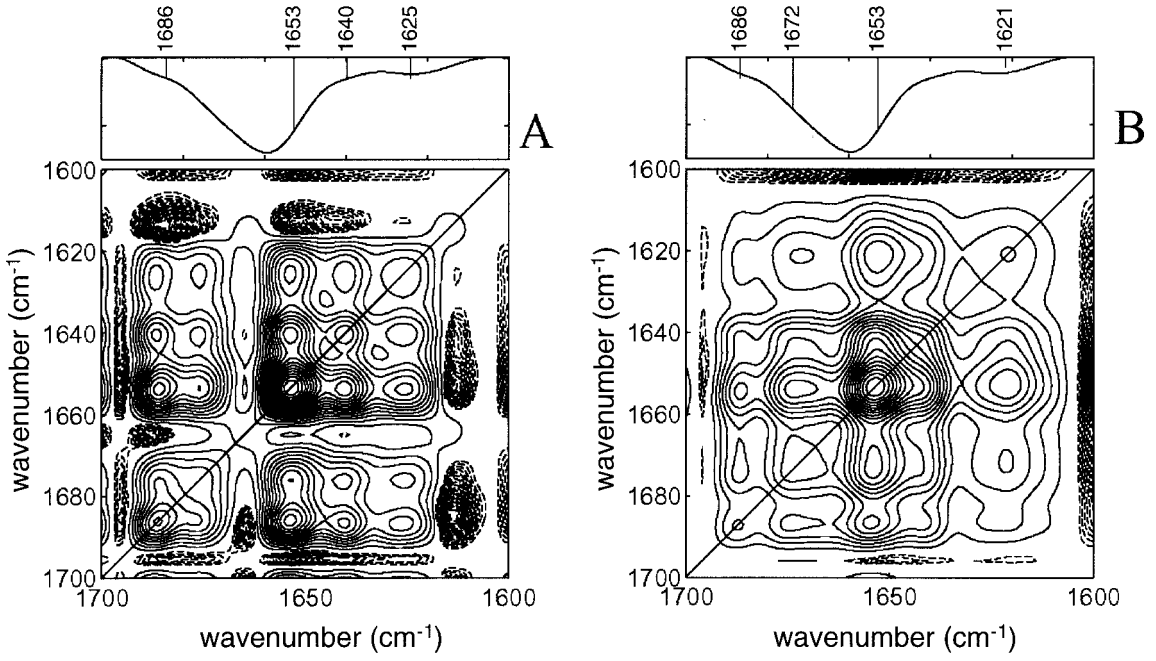

FIGURE 6 Synchronous 2D IR correlation plots of the monolayer IRRAS spectra of DPPG/SP-B (20:1, mol:mol, ~22 wt% SP-B). Solid lines indicate regions of positive correlation intensity; dashed lines indicate regions of negative correlation intensity. Spectra were divided into two pressure regions based on their autocorrelation intensities. 2D IR synchronous correlations were calculated on spectra contained within the pressure region. The one-dimensional spectrum shown in this figure is the calculated average of the spectra used in the 2D analysis. (*A*) 4.0–25.0 mN/m. (*B*) 25.0–40.0 mN/m.

1653 versus 1640 and 1625 cm^{-1}. In addition, a number of positive cross-peaks are formed between the β-structure bands at 1685 and 1676 cm^{-1} versus 1653, 1640, and 1625 cm^{-1}. Negative cross-peaks occur with the band at 1611 cm^{-1}. However, as in the case of SP-C, the peak at this wavenumber is most likely due to side-chain vibrations unrelated to protein secondary structure.

The high surface pressure region (25 mN/m) of the DPPG/SP-B monolayer presents a simpler correlation map than does the low-pressure region because it is dominated by the major α-helical auto peak at 1653 cm^{-1} (Fig. 6 *B*). There are additional auto peaks at 1686, 1672, and 1621 cm^{-1}, whereas positive cross-peaks can be observed at wavenumber values 1653 versus 1621 cm^{-1}, 1676 versus 1653 and 1621 cm^{-1}, and 1685 versus 1653 cm^{-1}.

The cross-peaks seen in the 2D synchronous spectra of DPPG/SP-B are very similar in wavenumber to the synchronous cross-peaks calculated for SP-C, indicating a high helical content for SP-B with contributions from β-sheet and unordered structure. These types of secondary structures have previously been observed in bulk phase IR studies of SP-B or the truncated N-terminal peptide of SP-B (Vandenbussche et al., 1992; Gordon et al., 2000). Also evident in the 2D spectra are the 1620/1685 cm^{-1} bands attributable to extended β-aggregated structures. These extended β-structures bands have not been seen in either the previous bulk phase studies or the IRRAS studies of SP-B mentioned above. The synchronous 2D IR spectrum of SP-B mainly differs from that of SP-C in that, for SP-B, the 2D correlations become less numerous at high surface pressures and are dominated by the α-helix band at 1653 cm^{-1}.

Asynchronous 2D IR correlation maps were also calculated from the DPPG/SP-B IRRAS monolayer spectra. Figure 7 shows the 2D contour map for the asynchronous correlation of the DPPG/SP-B spectra, in both the low surface pressure regime below 25 mN/m (Fig. 7 *A*) and the high surface pressure region above 25 mN/m (Fig. 7 *B*). The asynchronous 2D IR map of SP-B also indicates the presence of a heterogeneous secondary structure for this protein in the DPPG/SP-B monolayer film.

In the low-pressure region (Fig. 7 *A*) several prominent cross-peaks are observed that demonstrate the ability of asynchronous 2D IR to resolve overlapped peaks. Most noticeable is the fact that the prominent α-helix peak that occurs at 1653 cm^{-1} in the low-pressure synchronous spectrum of SP-B (Fig. 6 *A*) splits into two components in the low-pressure asynchronous spectrum (Fig. 7 *A*), one at 1656 and one at 1649 cm^{-1}. Both of these α-helix components generate asynchronous cross-peaks at wavenumber values characteristic of other secondary-structure conformations. For example, asynchronous cross-peaks are seen between 1649 cm^{-1} and (1640, 1628, 1690, 1676, and 1656 cm^{-1}). The higher wavenumber α-helix component at 1656 cm^{-1} also generates cross-peaks with 1682 and 1615 cm^{-1}. In addition, the extended β-sheet band observed at 1686 cm^{-1} in the low-pressure synchronous spectrum also splits into

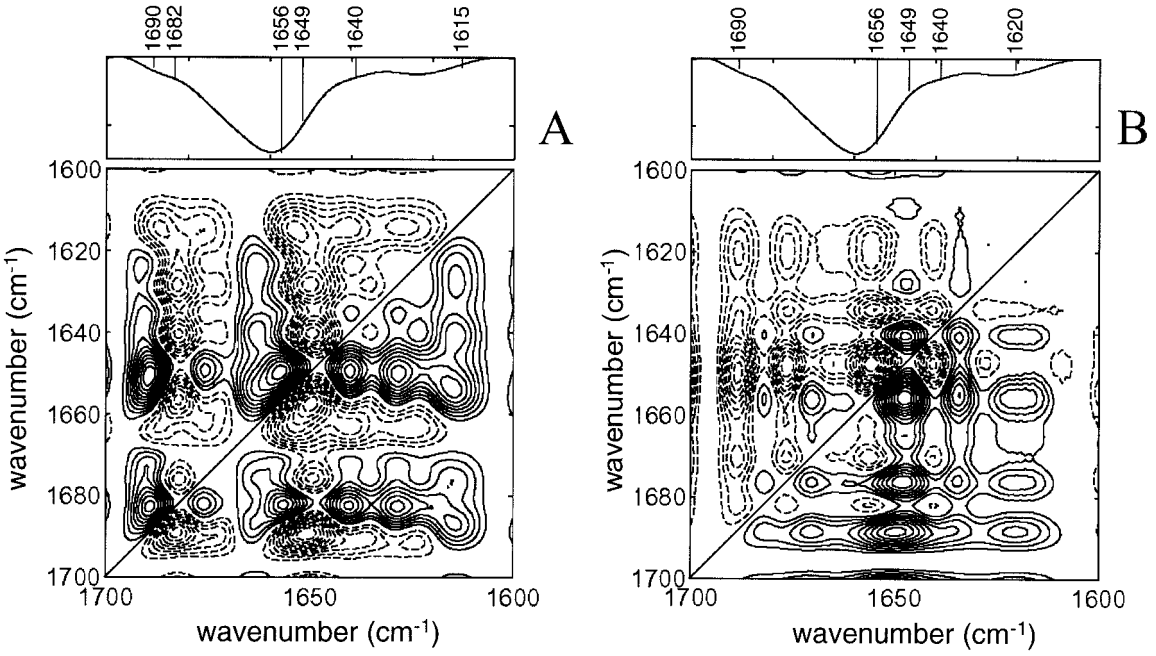

FIGURE 7 Asynchronous 2D IR correlation plots of the monolayer IRRAS spectra of DPPG/SP-B (40:1, mol:mol, ~22 wt% SP-B). Solid lines indicate regions of positive correlation intensity; dashed lines indicate regions of negative correlation intensity. Spectra were divided into two pressure regions based on their autocorrelation intensities. 2D IR asynchronous correlations were calculated on spectra contained within the pressure region. The one-dimensional spectrum shown in this figure is the calculated average of the spectra used in the 2D analysis. (*A*) 4.0–25.0 mN/m. (*B*) 25.0–40.0 mN/m.

lower and higher frequency components in the asynchronous spectrum (at 1682 and 1690 cm^{-1}, respectively). A number of additional prominent cross-peaks are seen at 1640 cm^{-1}, characteristic of unordered structures. Cross-peaks are observed between the extended β-sheet split components and other bands, including 1682 cm^{-1} and (1676, 1640, 1628, and 1690 cm^{-1}) and between 1690 cm^{-1} and (1615, 1624, and 1637 cm^{-1}).

The presence of two α-helix components in the 2D IR correlation spectrum for SP-B is consistent with previous IR results based on curve-fitting of the amide I region in the ATR spectra of bulk phase lipid/SP-B vesicles (Vandenbussche et al., 1992). This previous study attributed two amide I band components to two separate populations of α-helix in SP-B, a hydrophobic fraction associated with the lipid chains and a hydrophilic fraction parallel to the membrane surface. Presumably, the more hydrophilic fraction would encounter stronger H-bond potential with the aqueous solvent, thus slightly reducing its amide I frequency (i.e., the 1649-cm^{-1} peak is likely associated with the hydrophilic fraction). In Fig. 7 *A*, the distribution of correlation intensity between the two α-helix cross-peaks indicates that the protein exists primarily in the 1656-cm^{-1} hydrophobic fraction at low surface pressures. This current study is the first time that two α-helix fractions have been observed for SP-B in monomolecular films at the A/W interface.

The asynchronous map for DPPG/SP-B reveals that the splitting of the α-helix band into two cross-peaks persists in the high-pressure region above 25 mN/m (Fig. 7 *B*). However, the distribution of correlation intensity is reversed at high surface pressures. Above 25 mN/m, the main correlation intensity (and the sign of this cross-peak) has shifted and is now concentrated in the 1649-cm^{-1} component. The asynchronous correlation of the two amide I components results in a number of cross-peaks. The 1649-cm^{-1} α-helix band results in cross-peaks with (1640 and 1628 cm^{-1}), whereas the 1656-cm^{-1} helix component shows cross-peaks with 1649, 1634, and 1620 cm^{-1}. The extended β-sheet structure at 1690 cm^{-1} results in a long correlation-intensity minimum with cross-peaks at 1670, 1648 and 1620 cm^{-1}. Other prominent cross-peaks are seen between 1676 cm^{-1} and (1670, 1648, 1634, and 1620 cm^{-1}) and between 1682 cm^{-1} and (1676, 1656, and 1640 cm^{-1}).

$\beta\nu$ Correlation analysis of the SP-B amide I region

To quantitatively address how the different secondary structural components in SP-B respond with respect to increasing monolayer surface pressure, we have calculated the $\beta\nu$ correlation map for the IRRAS spectra of the DPPG/SP-B monolayer. The $\beta\nu$ plot for the amide I region of SP-B at low surface pressure (<25 mN/m) is shown in Fig. 8 *A* with the band assignments for these peaks and the values for their effective phase angle ($\beta_{e)}$ presented in Table 2. Figure 8 *A* shows that the most intense peak in the low-pressure $\beta\nu$ plot

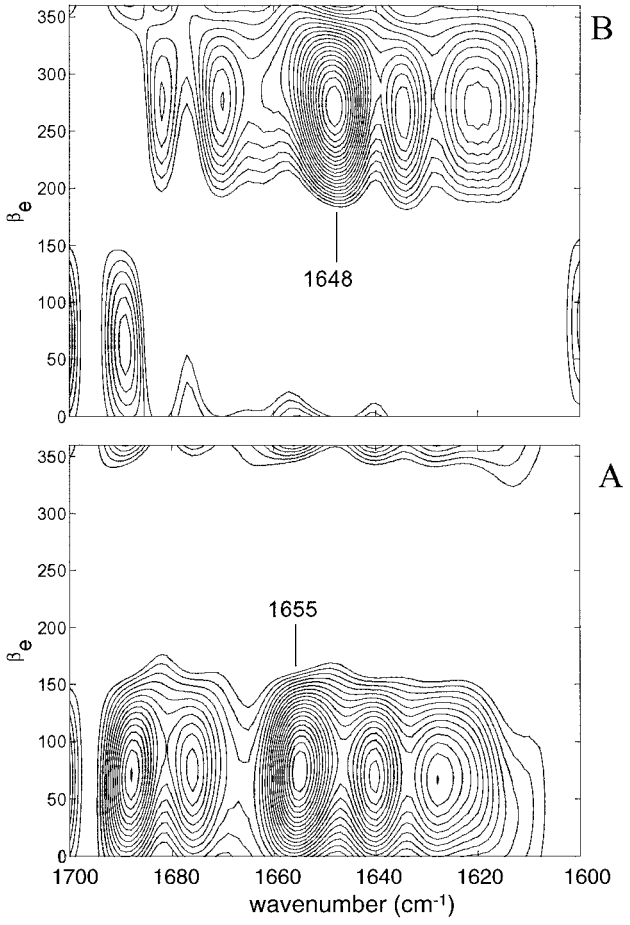

FIGURE 8 $\beta\nu$ Correlation plots derived from the monolayer IRRAS spectra of DPPG/SP-B (40:1, mol:mol, ~22 wt% SP-B). Spectra were divided into two pressure regions based on their autocorrelation intensities. $\beta\nu$ Correlations were calculated on spectra contained within the pressure region. (*A*) 4.0–25.0 mN/m. (*B*) 25.0–40.0 mN/m.

for SP-B is observed at 1655 cm^{-1} and corresponds to the α-helix. The wavenumber value for this peak in the $\beta\nu$ plot indicates that it corresponds to the 1656-cm^{-1} α-helix cross-peak seen in the asynchronous 2D IR correlation plot for SP-B (Fig. 7). This α-helix asynchronous cross-peak may be assigned to the hydrophobic helix fraction of SP-B. Peaks due to β structure (1628, 1676, and 1688 cm^{-1}) and to unordered structure (1640 cm^{-1}) are also apparent in the $\beta\nu$ plot. As was the case with SP-C at low pressure (Fig. 5 *A* and Table 1), it is clear from Fig. 8 *A* and Table 2 that each of the amide I peaks for SP-B at low surface pressures have nearly identical β_e values, in this case with a standard error of less than 3% relative to the mean. Thus, the same interpretation holds for SP-B as for SP-C at low surface pressure: all conformations of the SP-B protein reorient at the identical relative rate as the surface pressure is increased to 25 mN/m.

Figure 8 *B* illustrates the relative reorientation of SP-B secondary structure at high surface pressures (25–40 mN/m). As detailed in Table 2, the $\beta\nu$ correlation peaks due to different SP-B secondary structures have nearly identical β_e values at high pressures, similar to the situation at low surface pressure. The most intense correlation peak for SP-B at high surface pressures is that of the 1648-cm^{-1} peak with $\beta_e = 270.9$, attributable to the α-helix. The wavenumber value for this peak in the $\beta\nu$ plot indicates that it corresponds to the 1649-cm^{-1} α-helix cross-peak seen in the asynchronous 2D IR correlation plot for SP-B (Fig. 7). This α-helix asynchronous cross-peak may be assigned to the hydrophilic helix fraction of SP-B. Four other secondary structure $\beta\nu$ correlation peaks for SP-B at high surface pressures have nearly identical effective phase angles with the 1648-cm^{-1} helix peak (a standard error of less than 1% relative to the mean), indicating a nearly simultaneous reorientation for all protein segments. Theses peaks include 1682 cm^{-1} ($\beta_e = 277.2$), 1670 cm^{-1} ($\beta_e = 274.7$), 1634 cm^{-1} ($\beta_e = 266.0$), and 1620 cm^{-1} ($\beta_e = 272.2$), all of which can be attributed to β-sheet structures. A correlation peak at 1689 cm^{-1} ($\beta_e = 62.9$) is the only peak that does not fit this pattern. It reflects an extended β structure that reorients at a much slower relative rate than all the other protein segments in SP-B.

The 2D IR and $\beta\nu$ correlation methods lead to the following model for SP-B reorientation. At low surface pressures, SP-B is dominated by an α-helix secondary structure, however, the helix exists in two separate but coexisting conformations, one hydrophobic and one hydrophilic. Although both helix conformations coexist at low surface pressure, the hydrophobic conformation predominates. SP-B also has significant contributions from extended β-sheet and unordered structures. With increasing surface pressure, all conformations of the SP-B protein react identically and reorient in phase with each other. Above 25 mN/m, however, the intensity of the helix bands shifts, and the correlations are dominated by the α-helix-band charac-

TABLE 2 Effective phase angle, β_e, values calculated for DPPG/SP-B monolayer IRRAS spectra in amide I region

Wavenumber (cm^{-1})	β_e Value	Assignment
Region A: 4.0–25.0 mN/m		
1688.0	69.1	β strand (aggregated)
1676.2	75.4	β turn/loop
1654.8	74.1	α helix
1640.4	69.1	Unordered
1627.7	65.4	β strand (aggregated)
Region B: 25.0–40.0 mN/m		
1689.1	62.9	β strand (aggregated)
1681.8	277.2	β turn/loop
1670.0	274.7	β turn/loop
1648.0	270.9	α helix
1634.5	266.0	β sheet
1620.0	272.2	β strands (aggregated)

β_e Values taken from the $\beta\nu$ 2D correlation plots for the DPPG/SP-B monolayer (Figure 8).

teristic of the hydrophilic helix conformation. Both the 2D and $\beta\nu$ correlations detect the change in correlation intensity of the SP-B helix fractions with increasing surface pressure. Above 25 mN/m, β-sheet and unordered structures persist, but their correlation intensities decrease, leaving the hydrophilic α-helix as the dominant conformation. All SP-B conformations react identically to increasing surface pressure, leading to a reorientation of the protein subunits in phase with one another. The one exception to this concerted reorientation is that of an isolated extended β-structure peak, which lags significantly behind the reorientation rates of the other protein segments. The conservation of secondary structure and in-phase reorientation of the entire protein throughout all surface pressures is likely due to the stabilization of the SP-B protein core by its intramolecular disulfide bonds (Hawgood et al., 1998).

CONCLUSIONS

Using in situ IR spectroscopy at the A/W interface, we have investigated the conformational intermediates that exist in the hydrophobic surfactant proteins SP-B and SP-C in lipid–protein monolayers. To accomplish this, we have applied 2D IR and $\beta\nu$ correlation spectroscopy to the analysis of the protein amide I vibrations. The results described here have identified specific protein conformations and followed the reorientation of these protein conformations as a function of increasing surface pressure. Our conclusions are as follows. The surface pressure regimes that encompassed the greatest variation in amide I spectral intensity were identified using a statistical approach based on a windowed autocorrelation method. These regions were located by adapting a dynamic filtering technique that auto correlates IR intensities within a defined surface-pressure window and plots them against the average surface pressure, thereby locating the regions of maximal spectral variation. For both SP-B and SP-C, this autocorrelation method defined two separate surface-pressure regions that produced maximum amide I intensity changes: 4–25 mN/m and 25–40 mN/m. 2D IR and $\beta\nu$ correlation analyses were performed solely within these regions to establish the structural or temporal relationships that contributed to the spectral variations.

Multiple cross-peaks observed in the 2D IR correlation spectra demonstrate that SP-C is comprised of a heterogeneous secondary structure, including α-helix, β-sheet, and an intermolecular aggregation of extended β-sheet structure. The asynchronous spectrum shows that the main α-helix band splits into two peaks at high surface pressures, indicating that two different helix conformations exist for SP-C. This is the first IR evidence that multiple α-helix conformations and β-structure conformational intermediates exist for SP-C-containing monolayers at the A/W interface. At low surface pressures, SP-C exists in a variety of secondary structure conformations, most noticeably the predominate α-helix, but also including extended β-sheet structures. All conformations of the SP-C molecule react identically to increasing surface pressure and reorient in phase with each other. Above 25 mN/m, however, the increasing surface pressure selectively affects the coexisting protein conformations and leads to an independent reorientation of the protein subunits. The higher wavenumber α-helix conformation reorients first, closely followed by that of the extended β structures, including that of the aggregated protein strands. The slowest protein motion originates from the dominant α-helix conformation and from β turn/loop structures. It is possible that the independent reorientation of the two α-helix conformations plays a role in the SP-C-mediated formation of three-dimensional, surface-associated, lipid–protein structures.

The 2D synchronous spectra of DPPG/SP-B indicate a high α-helical content for SP-B with contributions from β-sheet and unordered structure. The asynchronous 2D IR spectrum of SP-B shows that the prominent α-helix peak occurring at 1653 cm^{-1} in the synchronous spectrum splits into two components, one at 1656 and one at 1649 cm^{-1}. The presence of two α-helix components in the 2D IR correlation spectrum for SP-B is consistent with two separate populations of α-helix in SP-B, a hydrophobic fraction associated with the lipid chains and a hydrophilic fraction parallel to the membrane surface. This is the first study to demonstrate the presence of two α-helical components of SP-B in monomolecular films at the A/W interface. The distribution of correlation intensity between the two α-helix cross-peaks indicates that the protein exists primarily in the hydrophobic fraction at low surface pressures. The splitting of the α-helix band into two cross-peaks persists in the high-pressure region above 25 mN/m. However, at high surface pressures the correlation intensity of the helix bands reverses, and the 2D spectra are dominated by the α-helix band characteristic of the hydrophilic helix conformation. Both the 2D and $\beta\nu$ correlations detect the change in correlation intensity of the amide I α-helix bands with increasing surface pressure. With increasing surface pressure, all conformations of the SP-B protein react identically and reorient in phase with each other. Above 25 mN/m, β-sheet and unordered structures persist, but their correlation intensities decrease, leaving the hydrophilic α-helix as the dominant conformation. The conservation of protein secondary structure and in-phase reorientation of the entire protein throughout all surface pressures is likely due to the stabilization of the protein core by intramolecular disulfide bonds.

The work described here was supported by the U.S. Public Health Service through National Institutes of Health grant GM40117 (R.A.D.).

REFERENCES

Avery, M. E., and J. Mead. 1959. Surface properties in relation to atelectasis and hyaline membrane disease. *Am. J. Dis. Child.* 97:517–523.

Baatz, J. E., B. Elledge, and J. A. Whitsett. 1990. Surfactant protein SP-B induces ordering at the surface of model membrane bilayers. *Biochemistry.* 29:6714–6720.

Baatz, J. E., Y. Zou, J. T. Cox, Z. Wang, and R. H. Notter. 2001. High yield purification of lung surfactant proteins SP-B and SP-C and the effects on surface activity. *Protein Express. Purificat.* 23:180–190.

Berry, R. J., and Y. Ozaki. 2001. Investigation into the effect of instrumental parameters in two-dimensional correlation spectroscopy. *Appl. Spectrosc.* 55:1092–1098.

Bourdos, N., F. Kollmer, A. Benninghoven, M. Ross, M. Sieber, and H. J. Galla. 2000. Analysis of lung surfactant model systems with time-of-flight secondary ion mass spectrometry. *Biophys. J.* 79:357–369.

Byler, D. M., and H. Susi. 1986. Examination of the secondary structure of proteins by deconvolved FTIR spectra. *Biopolymers.* 25:469–487.

Cameron, D. G., J. K. Kauppinen, and D. Moffatt. 1982. Precision in condensed phase vibrational spectroscopy. *Appl. Spectrosc.* 36:245–250.

Chen, P. S., T. Y. Toriba, and H. Warner. 1956. Microdetermination of phosphorous. *Anal. Chem.* 28:1756–1758.

Creuwels, L. A. J. M., L. M. G. van Golde, and H. P. Haagsman. 1997. The pulmonary surfactant system: biochemical and clinical aspects. *Lung.* 175:1–39.

Ding, J., D. Y. Takamoto, A. von Nahmen, M. M. Lipp, K. Y. C. Lee, A. Waring, and J. A. Zasadzinski. 2001. Effects of lung surfactant proteins, SP-B and SP-C, and palmitic acid on monolayer stability. *Biophys. J.* 80:2262–2272.

Discher, B. M., W. R. Schief, V. Vogel, and S. B. Hall. 1999. Phase separation in monolayers of pulmonary surfactant phospholipids at the air–water interface: composition and structure. *Biophys. J.* 77: 2051–2061.

Dluhy, R. A. 1986. Quantitative external reflection infrared spectroscopic analysis of insoluble monolayers spread at the air–water interface. *J. Phys. Chem.* 90:1373–1379.

Dluhy, R. A. 2000. Infrared spectroscopy of biophysical monolayer films at interfaces. Theory and applications. *In*: Physical Chemistry of Biological Interfaces. A. Baszkin, W. Norde, editors. Marcel Dekker, New York. 711–747.

Dluhy, R. A., K. E. Reilly, R. D. Hunt, M. L. Mitchell, A. J. Mautone, and R. Mendelsohn. 1989. Infrared spectroscopic investigations of pulmonary surfactant. Surface film transitions at the air–water interface and bulk phase thermotropism. *Biophys. J.* 56:1173–1181.

Elmore, D. L., and R. A. Dluhy. 2000a. Application of 2D IR correlation analysis to phase transitions in Langmuir monolayer films. *Colloids and Surfaces A.* 171:225–239.

Elmore, D. L., and R. A. Dluhy. 2000b. Pressure-dependent changes in the infrared C-H vibrations of monolayer films at the air/water interface revealed by two-dimensional infrared correlation spectroscopy. *Appl. Spectrosc.* 54:956–962.

Elmore, D. L., and R. A. Dluhy. 2001. $\beta\nu$ Correlation analysis: a modified two-dimensional infrared correlation method for determining relative rates of intensity change. *J. Phys. Chem. B* 105:11377–11386.

Elmore, D. L., S. Shanmukh, and R. A. Dluhy. 2002. A study of binary phospholipid mixtures at the air–water interface using infrared reflection–absorption spectroscopy and 2D-IR $\beta\nu$ correlation analysis. *J. Phys. Chem. A.* In Press.

Filosa, A., Y. Wang, A. A. Ismail, and A. M. English. 2001. Two-dimensional infrared correlation spectroscopy as a probe of sequential events in the thermal unfolding of cytochromes *c*. *Biochemistry.* 40: 8256–8263.

Flach, C. R., A. Gericke, K. M. W. Keough, and R. Mendelsohn. 1999. Palmitoylation of lung surfactant protein SP-C alters surface thermodynamics, but not protein secondary structure or orientation in 1,2-dipalmitoylphosphatidylcholine Langmuir films. *Biochim. Biophys. Acta.* 1416:11–20.

Galla, H. J., N. Bourdos, A. von Nahmen, M. Amrein, and M. Sieber. 1998. The role of pulmonary surfactant protein C during the breathing cycle. *Thin Solid Films.* 329:632–635.

Gericke, A., C. R. Flach, and R. Mendelsohn. 1997. Structure and orientation of lung surfactant SP-C and L-α-dipalmitoylphosphatidylcholine in aqueous monolayers. *Biophys. J.* 73:492–499.

Goormaghtigh, E., V. Cabiaux, and J.-M. Ruysschaert. 1994. Determination of soluble and membrane protein structure by Fourier transform infrared spectroscopy. I. Assignments and model compounds. *In*: Physiochemical Methods in the Study of Biomembranes. H. J. Hilderson, G. B. Ralston, editors. Plenum Press, New York. 329–362.

Gordon, L. M., K. Y. C. Lee, M. M. Lipp, J. A. Zasadzinski, F. J. Walther, M. A. Sherman, and A. J. Waring. 2000. Conformational mapping of the N-terminal segment of surfactant protein B in lipid using C-13-enhanced Fourier transform infrared spectroscopy. *J. Peptide Res.* 55:330–347.

Graff, D. K., B. Pastrana-Rios, S. Y. Venyaminov, and F. G. Prendergast. 1997. The effects of chain length and thermal denaturation on helix-forming peptides: a mode-specific analysis using 2D FT-IR. *J. Am. Chem. Soc.* 119:11282–11294.

Gustafsson, M., J. Thyberg, J. Naslund, E. Eliasson, and J. Johansson. 1999. Amyloid fibril formation by pulmonary surfactant protein C. *FEBS Lett.* 464:138–142.

Harrington, P. d. B., A. Urbas, and P. J. Tandler. 2000. Two-dimensional correlation analysis. *Chemom. Intel. Lab. Syst.* 50:149–174.

Hawgood, S., B. J. Benson, J. Schilling, D. Damm, J. A. Clements, and R. T. White. 1987. Nucleotide and amino acid sequences of pulmonary surfactant protein SP 18 and evidence for cooperation between SP 18 and SP 28–36 in surfactant lipid adsorption. *Proc. Natl. Acad. Sci. U.S.A.* 84:66–70.

Hawgood, S., M. Derrick, and P. Poulain. 1998. Structure and properties of surfactant protein B. *Biochim. Biophys. Acta.* 1408:150–160.

Hawgood, S., and K. Schiffer. 1991. Structures and properties of the surfactant-associated proteins. *Annu. Rev. Physiol.* 53:375–394.

Holm, B. A., Z. Wang, E. A. Egan, and R. H. Notter. 1996. Content of dipalmitoyl phosphatidylcholine in lung surfactant: ramifications for surface activity. *Pediatr. Res.* 39:805–811.

Hunt, A. N., F. J. Kelly, and A. D. Postle. 1991. Developmental variation in whole human lung phosphatidylcholine molecular species: a comparison of guinea pig and rat. *Early Hum. Develop.* 25:157–171.

Ismoyo, F., Y. Wang, and A. A. Ismail. 2000. Examination of the effect of heating on the secondary structure of avidin and avidin–biotin complex by resolution-enhanced two-dimensional infrared correlation spectroscopy. *Appl. Spectrosc.* 54:939–947.

Jackson, M., and H. H. Mantsch. 1995. The use and misuse of FTIR spectroscopy in the determination of protein structure. *Crit. Rev. Biochem. Mol. Biol.* 30:95–120.

Johansson, J., T. Curstedt, and B. Robertson. 1994a. The proteins of the surfactant system. *Eur. Respir. J.* 7:372–391.

Johansson, J., T. Szyperski, T. Curstedt, and K. Wüthrich. 1994b. The NMR structure of the pulmonary surfactant-associated polypeptide SP-C in an apolar solvent contains a valyl-rich α-helix. *Biochemistry.* 33: 6015–6023.

Kahn, M. C., G. J. Anderson, W. R. Anyan, and S. B. Hall. 1995. Phosphotidylcholine molecular species of calf lung surfactant. *Am. J. Physiol.* 13:L567–L573.

Khurana, R., and A. L. Fink. 2000. Do parallel β-helix proteins have a unique Fourier transform infrared spectrum? *Biophys. J.* 78:994–1000.

Kramer, A., A. Wintergalen, M. Sieber, H. J. Galla, M. Amrein, and R. Guckenberger. 2000. Distribution of the surfactant-associated protein C within a lung surfactant model film investigated by near-field optical microscopy. *Biophys. J.* 78:458–465.

Krol, S., A. Janshoff, M. Ross, and H. J. Galla. 2000. Structure and function of surfactant protein B and C in lipid monolayers: a scanning force microscopy study. *Phys. Chem. Chem. Phys.* 2:4586–4593.

Krüger, P., M. Schalke, Z. Wang, R. H. Notter, R. A. Dluhy, and M. Lösche. 1999. Effect of hydrophobic surfactant peptides SP-B and SP-C on binary phospholipid monolayers. I. Fluorescence and dark-field microscopy. *Biophys. J.* 77:903–914.

Kubelka, J., and T. A. Keiderling. 2001. Differentiation of β-sheet-forming structures: ab initio-based simulations of IR absorption and vibrational

CD for model peptides and protein β-sheets. *J. Am. Chem. Soc.* 123: 12048–12058.

Kubelka, J., P. Pancoska, and T. A. Keiderling. 1999. Novel use of a static modification of two-dimensional correlation analysis. Part II: heterospectral correlations of protein, Raman, FT-IR and circular dichroism spectra. *Appl. Spectrosc.* 53:666–671.

Lewis, J. F., and A. H. Jobe. 1993. Surfactant and the adult respiratory distress syndrome. *Am. Rev. Respir. Dis.* 147:218–233.

Mendelsohn, R., J. W. Brauner, and A. Gericke. 1995. External infrared reflection-absorption spectrometry. Monolayer films at the air–water interface. *Ann. Rev. Phys. Chem.* 46:305–334.

Morrissey, J. H. 1981. Silver stain for proteins in polyacrylamide gels: a modified procedure with enhanced uniform sensitivity. *Anal. Biochem.* 117:307–310.

Murayama, K., Y. Wu, B. Czarnik-Matusewicz, and Y. Ozaki. 2001a. Two-dimensional/attenuated total reflection infrared correlation spectroscopy studies on secondary structural changes in human serum albumin in aqueous solutions: pH-dependent structural changes in the secondary structures and in the hydrogen bondings of side chains. *J. Phys. Chem. B* 105:4763–4769.

Murayama, K., Y. Wu, B. Czarnik-Matusewicz, and Y. Ozaki. 2001b. Two-dimensional/attenuated total reflection infrared correlation spectroscopy studies on secondary structural changes in human serum albumin in aqueous solutions: pH-dependent structural changes in the secondary structures and in the hydrogen bondings of side chains. *J. Phys. Chem. B* 105:4763–4769.

Nabet, A., and M. Pezolet. 1997. Two-dimensional FT-IR spectroscopy: a powerful method to study secondary structure of proteins using H-D exchange. *Appl. Spectrosc.* 51:466–469.

Noda, I. 1990. Two-dimensional infrared (2D IR) spectroscopy: theory and applications. *Appl. Spectrosc.* 44:550–554.

Noda, I. 1993a. Generalized two-dimensional correlation method applicable to infrared, Raman, and other types of spectroscopy. *Appl. Spectrosc.* 47:1329–1336.

Noda, I. 1993b. Recent developments in two-dimensional infrared (2D IR) correlation spectroscopy. *Appl. Spectrosc.* 47:1317–1323.

Noda, I. 2000. Determination of two-dimensional correlation spectra using the Hilbert transform. *Appl. Spectrosc.* 54:994–999.

Noda, I., A. E. Dowrey, C. Marcott, G. M. Story, and Y. Ozaki. 2000. Generalized two-dimensional correlation spectroscopy. *Appl. Spectrosc.* 54:236A–248A.

Noda, I., G. M. Story, and C. Marcott. 1999. Pressure-induced transitions of polyethylene studied by two-dimensional infrared correlation spectroscopy. *Vib. Spectrosc.* 19:461–465.

Notter, R. H. 1984. Surface chemistry of pulmonary surfactant: the role of individual components. *In*: Pulmonary Surfactant. B. Robertson, L. G. M. van Golde, J. J. Battenburg, editors. Elsevier, Amsterdam. 17–53.

Notter, R. H. 2000. Lung Surfactants: Basic Science and Clinical Applications. Marcel Dekker, Inc., New York.

Notter, R. H., and Z. Wang. 1997. Pulmonary surfactant: physical chemistry, physiology and replacement. *Rev. Chem. Eng.* 13:1–118.

Oosterlaken-Dijksterhuis, M. A., H. P. Haagsman, L. M. G. v. Golde, and R. A. Demel. 1991. Characterization of lipid insertion into monomolecular layers mediated by lung surfactant proteins SP-B and SP-C. *Biochemistry.* 30:10965–10971.

Ozaki, Y., and I. Noda, editors. 2000. Two-Dimensional Correlation Spectroscopy. American Institute of Physics, New York.

Pancoska, P., J. Kubelka, and T. A. Keiderling. 1999. Novel use of a static modification of two-dimensional correlation analysis. Part I. Comparison of the secondary structure sensitivity of electronic circular dichroism, FT-IR, and Raman spectra of proteins. *Appl. Spectrosc.* 53: 655–665.

Paquet, M. J., M. Laviolette, M. Pezolet, and M. Auger. 2001. Two-dimensional infrared correlation spectroscopy study of the aggregation of cytochrome *c* in the presence of dimyristoylphosphatidylglycerol. *Biophys. J.* 81:305–312.

Pastrana-Rios, B., S. Taneva, K. M. W. Keough, A. J. Mautone, and R. Mendelsohn. 1995. External reflection absorption infrared spectroscopy study of lung surfactant proteins SP-B and SP-C in phospholipid monolayers at the air/water interface. *Biophys. J.* 69:2531–2540.

Pison, U., W. Seeger, R. Buchhorn, T. Joka, M. Brand, U. Obertacke, H. Neuhof, and K. P. Schmit-Nauerburg. 1989. Surfactant abnormalities in patients with respiratory failure after multiple trauma. *Am. Rev. Respir. Dis.* 140:1033–1039.

Schultz, C. P., O. Barzu, and H. H. Mantsch. 2000. Two-dimensional infrared correlation analysis of protein unfolding: use of spectral simulation to validate structural changes during thermal denaturation of bacterial CMP kinases. *Appl. Spectrosc.* 54:931–938.

Sefara, N. L., N. P. Magtoto, and H. H. Richardson. 1997. Structural characterization of β-lactoglobulin in solution using two-dimensional FT mid-infrared and FT near-infrared correlation spectroscopy. *Appl. Spectrosc.* 51:536–540.

Shin, Y. S. 1962. Spectrophotometric ultramicrodetermination of inorganic phosphorus and lipid phosphorus in serum. *Anal. Chem.* 34:1164–1166.

Surewicz, W. K., H. H. Mantsch, and D. Chapman. 1993. Determination of protein secondary structure by Fourier transform infrared spectroscopy: a critical assessment. *Biochemistry.* 32:7720–7726.

Szyperski, T., G. Vandenbussche, T. Curstedt, J. M. Ruysschaert, K. Wuthrich, and J. Johansson. 1998. Pulmonary surfactant-associated polypeptide C in a mixed organic solvent transforms from a monomeric α-helical state into insoluble β-sheet aggregates. *Protein Sci.* 7:2533–2540.

Takamoto, D. Y., M. M. Lipp, A. von Nahmen, K. Y. C. Lee, A. Waring, and J. A. Zasadzinski. 2001. Interaction of lung surfactant proteins with anionic phospholipids. *Biophys. J.* 81:153–169.

Taneva, S., and K. M. W. Keough. 1994a. Pulmonary surfactant proteins SP-B and SP-C in spread monolayers at the air–water interface: I. Monolayers of pulmonary surfactant protein SP-B and phospholipids. *Biophys. J.* 66:1137–1148.

Taneva, S., and K. M. W. Keough. 1994b. Pulmonary surfactant proteins SP-B and SP-C in spread monolayers at the air–water interface: II. Monolayers of pulmonary surfactant protein SP-C and phospholipids. *Biophys. J.* 66:1149–1157.

Taneva, S., and K. M. W. Keough. 1994c. Pulmonary surfactant proteins SP-B and SP-C in spread monolayers at the air–water interface: III. Proteins SP-B plus SP-C with phospholipids in spread monolayers. *Biophys. J.* 66:1158–1166.

Tchoreloff, P., A. Gulik, B. Denizot, J. E. Proust, and F. Puisieux. 1991. A structural study of interfacial phospholipid and lung surfactant layers by transmission electron microscopy after Blodgett sampling: influence of surface pressure and temperature. *Chem. Phys. Lipids.* 59:151–165.

Thomas, M., and H. H. Richardson. 2000. Two-dimensional FT-IR correlation analysis of the phase transition in a liquid crystal, 4′-*n*-octyl-4-cyanobiphenyl (8CB). *Vib. Spectrosc.* 24:137–146.

Vandenbussche, G., A. Clerx, M. Clerx, T. Curstedt, J. Johansson, H. Jornvall, and J. Ruysschaert. 1992. Secondary structure and orientation of the surfactant protein SP-B in a lipid environment: a Fourier transform infrared spectroscopy study. *Biochemistry.* 31:9169–9176.

Wang, Y., K. Murayama, Y. Myojo, R. Tsenkova, N. Hayashi, and Y. Ozaki. 1998. Two-dimensional Fourier transform near-infrared spectroscopy study of heat denaturation of ovalbumin in aqueous solution. *J. Phys. Chem. B.* 102:6655–6662.

Wang, Z., O. Gurel, J. E. Baatz, and R. H. Notter. 1996. Differential activity and lack of synergy of lung surfactant proteins SP-B and SP-C in interactions with phospholipids. *J. Lipid Res.* 37:1749–1760.